Int J Adv Manuf Technol (2018) 95:355–365
https://doi.org/10.1007/s00170-017-1179-z

ORIGINAL ARTICLE

Process planning for laser wire-feed metal additive manufacturing system

Yaoyu Ding[1] · **Meysam Akbari**[1] · **Radovan Kovacevic**[1]

Received: 19 June 2017 / Accepted: 27 September 2017 / Published online: 23 October 2017

Abstract Laser wire-feed metal additive manufacturing (LWMAM) is a promising additive manufacturing technology that is well suited to build from various materials near net shape mid- to large-size complex components with a high deposition rate and high material usage. It could find applications in diverse industrial sectors such as aerospace, automotive, oil and gas, and rapid tooling. To further gain the acceptance of this technology, the development of process planning software is identified as one of the main challenges. LWMAM has several specific features that complicate the process planning compared to other similar additive manufacturing processes. LWMAM is still in its infancy. In this study, key features involved in the LWMAM process were first identified by building a prismatic block. The corresponding strategies were proposed and tested. Then, a MATLAB-based process planning software was developed that consisted of modules for volume slicing, contour filling, track trimming/elongating, stair-step effect compensation, and post-processing. Free-form contours and a propeller were successfully built by using the developed software. The as-built shapes were measured and compared to the CAD models.

Keywords Laser · Wire · Metal additive manufacturing · Process planning · Stair-step · Propeller

✉ Radovan Kovacevic
kovacevi@lyle.smu.edu

[1] Department of Mechanical Engineering, Research Center for Advanced Manufacturing, Southern Methodist University, 3101 Dyer Street, Dallas, TX 75205, USA

1 Introduction

Metal additive manufacturing (AM) technologies [1], such as directed energy deposition (DED) [2] and powder bed AM processes [3], have been of great interest in industries due to their capability of fabricating functional components directly from CAD models. As one of the typical DED processes, laser wire-feed metal additive manufacturing (LWMAM) fabricates metal components by slicing the 3D CAD model into a set of two-dimensional (2D) layers, then depositing material to fill each layer by using metal wire as the feedstock and laser as the heat source. LWMAM has potential to build from various materials such as mild steel, stainless steel, Ni alloys [4, 5], Ti alloys [6, 7], and Al alloys near net shape mid- to large-size components from their CAD models with a high deposition rate and high material usage (almost 100%). These advantages have been attracting attention from different industrial sectors including aerospace, automotive, oil and gas, and rapid tooling. To further gain the acceptance of this technology, several main challenges have been identified including process planning software development, relatively poor surface quality, residual stress and distortion of buildups [8, 9], mechanical property optimization [10, 11], process monitoring, and control for stability and repeatability [12, 13]. The Research Center for Advanced Manufacturing (RCAM) at Southern Methodist University has been developing a robotized LWMAM system targeting solutions and improvements for those challenges [14]. This paper aims at the development of process planning software for LWMAM as an extension of the process planning software developed for laser powder-feed metal additive manufacturing (LPMAM) in RCAM [15].

Generally, process planning processes for metal additive manufacturing (MAM) with material feeding (laser wire-

feed MAM, arc wire-feed MAM [16], electron wire-feed MAM [17], and laser powder-feed MAM [18]) share some basic requirements:

(1) The number of start-and-stop points on the boundary of a layer are minimized to improve the surface quality and mitigate the stair-step effect,
(2) The number of tracks for filling a layer are minimized to save on the deposition time,
(3) An offsetting of the component boundary is considered to allow for machining/milling if a high shape accuracy is needed.

Compared to other material-feeding MAMs, LWMAM has specific requirements that further complicate the process planning process such as

(1) The best performance in terms of surface quality and deposition stability is achieved by feeding and placing wire at the leading edge of the molten pool [19–21]. The laser head must rotate in order to align the tangential direction of the deposition track. Consequently, areas at sharp corners cannot be covered continuously by a single deposition track, because a sharp direction change of the laser head will negatively affect the deposition stability and surface quality. The deposition track must be only a straight line or a smooth curve. This limitation significantly affects the choice of filling patterns for LWMAM.
(2) A number of problems could occur during the deposition on individual tracks like the wire sticking to the end of individual tracks, droplet formation at the end of the wire tip after finishing a track, and formation of a bump/wedge shape at the start-and-stop points of the individual tracks. These problems must be handled by coordinating the robot speed, laser power, and wire feeding rate at the start-and-stop points of individual tracks. The process planning software must specify the corresponding control strategies/parameters.

Some process planning software have been reported for arc wire-feed MAM [22–25] and laser powder-feed MAM [15, 26–28]. Dwivedi et al. [25] proposed a method that subdivided a 2D polygonal section into a set of monotone polygons and generated a continuous depositing track for a gas tungsten arc welding MAM system. That method improved the deposition surface by decreasing the number of start-and-stop points on the boundary of each layer. Zhang et al. [22] developed a process planning software for a gas metal arc welding (GMAW) MAM system that included modules for slicing the part, planning the deposition parameters, and controlling the deposition process. In this study, the outline of each layer was deposited first, and the interior of the sliced contour was filled with a raster filling pattern to obtain a high deposition speed. These methods worked well for arc wire-feed MAM but not for LWMAM because a sharp direction change of the laser head easily occurred during depositing the continuous track or the outline. In ref. [24], the process planning software sliced the STL file in a self-developed STL editor. The generated polygon data was imported into a NC post-processing software to generate the NC tool path. Those software dealt well with the corresponding MAM processes. However, at this stage, no process planning software has been reported to meet the specific requirements listed above for LWMAM. Most of the geometries built by LWMAM were geometrically simple or had regular shapes such as a single-bead wall, prismatic block [29], or cylinder [12]. For most of these geometries, the path was planned by teaching mode.

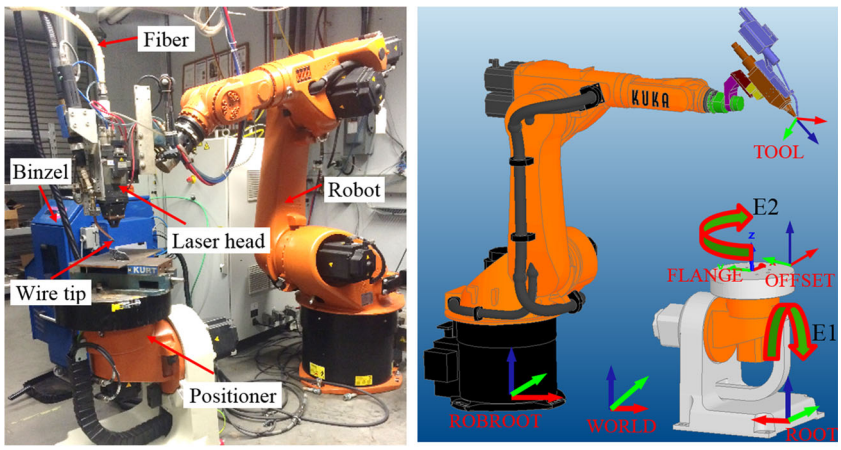

Fig. 1 **a** Photo of RLWAM system in RCAM. **b** Coordinate systems of six + two-axis robot system

Table 1 Chemical composition of filler wire Lincoln ER 100S-G

%C	%Mn	%Si	%Ni	%Mo	%Cr	%S	%P	%V	%Al	%Ti	%Zr	%Cu
0.05–0.06	1.63–1.69	0.46–0.50	1.88–1.96	0.43–0.45	0.04–0.06	0.002–0.005	0.005–0.009	<0.01	<0.01	0.03–0.04	<0.01	0.11–0.14

In this work, a robotized LWMAM system was developed in RCAM. A MATLAB -based process planning software was developed that consists of modules for volume slicing, contour filling, track trimming/elongating, stair-step effect compensation, and post-processing (for a KUKA robot).

The paper is organized as follows: Sect. 2 describes the setup of the robotized LWMAM system in RCAM. Section 3 details the key issues involved in building a prismatic block which is a fundamental step before building more complex geometries. Section 4 describes the process planning procedure for free-form contour and proposes a method to evaluate the shape accuracy and qualification of the as-built shape. To test the performance of the proposed process planning software, Sect. 5 describes the fabrication of a free-form contour and propeller; shape accuracies were also evaluated. Section 6 concludes the work in this paper.

2 Setup of LWMAM system

The photo and schematic view of the robotized LWMAM system are shown in Fig. 1a, b, respectively. A 4-kW fiber laser with a wavelength of 1070 nm along with a laser head is mounted on a KUKA six-axis robot arm to perform the metal deposition. The system is also equipped with a two-axis tilt and rotatory positioning system that is integrated with the six-axis robot arm. As shown in Fig. 1b, the TOOL coordinate system is located at the tool center point (TCP) that is the junction of the wire tip and the laser beam. Mild steel Lincoln ER 100S-G wire with diameter of 1.2 mm is chosen as the feedstock material. Table 1 lists the chemical composition of the wire. The wire is fed by a push-pull feeding device (ABICOR® BINZEL). One motor installed on the laser head pulls the wire while another motor in the feeder machine simultaneously pushes the wire. The wire-feeding torch is installed at 40° with respect to the laser beam. The wire stick-out is around 12 mm long. During the building process, the shielding gas (argon) is directed through the nozzle toward the molten pool to protect the molten material from the atmosphere.

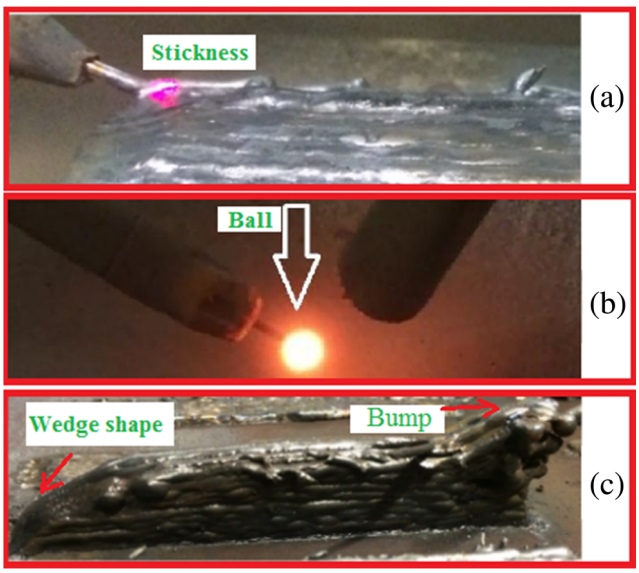

Fig. 2 Problems during building a block

3 Preliminary study: deposit a block

Several trials took place to deposit a single bead on the plate. The best performance in terms of surface quality and deposition stability was achieved by feeding and placing the wire at the leading edge of the molten pool. This process was in agreement with work published in refs. [19, 20]. It was also found that a sharp direction change of the laser head negatively affected the deposition stability and surface quality. Among the tool-path patterns including raster [30], zigzag [25], contour [31], spiral [32], continuous [33], and hybrid [22], only the raster pattern was feasible to be adopted by LWMAM. With the raster pattern, there was no need to sharply change the direction of the laser head. In this study, therefore, the raster pattern was chosen to generate the tool path for building up a prismatic

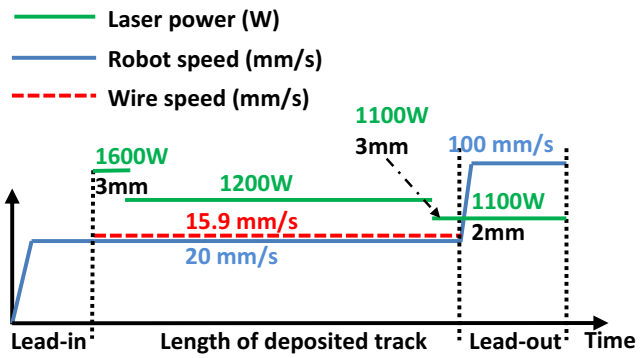

Fig. 3 Relationship among the laser power, robot speed, and wire-feed rate during depositing a track

Table 2 Processing parameters for building a block

Scanning speed (mm/s)	Laser powder (W)	Wire rate (mm/s)	*y* offset (mm)	*z* increment (mm)	Pull speed (mm/s)/ distance (mm)	Start laser distance (mm)/value (W)	End laser distance (mm)/value (W)
20	1200	15.9	1.25	0.5	100/2	3/1600	3/1000

block (see Fig. 4a). Later, a new tool-path pattern evolved from the raster pattern was proposed to build free-form structures.

During the LWMAM process, the wire was melted continuously by laser beam. The melted material flowed to the molten pool and solidified quickly as the laser head moved forward. After reaching the end of each individual track, the laser switched off, and the tip of the wire stuck to the end of the track due to the quick solidification of the molten pool (see Fig. 2a). This disruption severely inhibited the continuation of the building process and damaged the wire-feeding torch. To avoid this disruption, the motion of the laser head was programmed to travel a lead-out distance (2 mm) with a high speed (100 mm/s) at the end of the track such that the tip of the wire was pulled out of the molten pool before it solidified (see the phase of "lead-out" in Fig. 3). Due to the acceleration of the robot arm at the beginning of track, a lead-in phase was also added at the beginning of track. This lead-in ensured that the robot arm speed would reach scanning speed before the wire feeding and laser were turned on (see the phase of "lead-in" in Fig. 3). When the wire tip was pulled out from the molten pool, it removed some of the material from the molten pool. This material formed a ball at the end of the wire tip (see Fig. 2b). Consequently, a wedge shape was formed at the end of the block (see Fig. 2c). The ball was carried to the starting position of the next track that generated a bump at the starting position (see Fig. 2c). To eliminate the wedge shape and bump, the laser power was decreased at the place 3 mm before the end of track. The decrease insured a small molten pool. Therefore, when the wire tip was pulled out from the molten pool, just a small amount of material was removed. The size of the bump at the starting position of tracks decreased after the ball disappeared. Since the laser energy at the starting position of track was not large enough to make the molten pool expand sideways, a small bump still existed. By setting up a higher laser power at the start of track, the bump disappeared. Figure 3 shows the schematic of the operations and parameters of the laser power, wire-feed rate, and robot speed during the deposition of a track. A set of processing parameters is specified in Table 2 by trial and error. The *y* offset is the distance between adjacent tracks in one layer, and the *z* increment is the distance along *z* axis after finishing one layer. As shown in Fig. 4, blocks of 115 mm in height, 60 mm in length, and 10 mm in thickness were built by using the proposed procedure shown in Fig. 3 and the processing parameters shown in Table 2. The starting and ending positions of the tracks were uniform, and the sideway surface quality of the built blocks was smooth. Building good blocks laid a solid foundation for building free-form geometries.

4 Build free-form volume

4.1 Criteria of process planning

Solid components with free-form boundaries like propeller, blade, and impeller are widely used in different industrial sectors. By slicing those components from bottom to

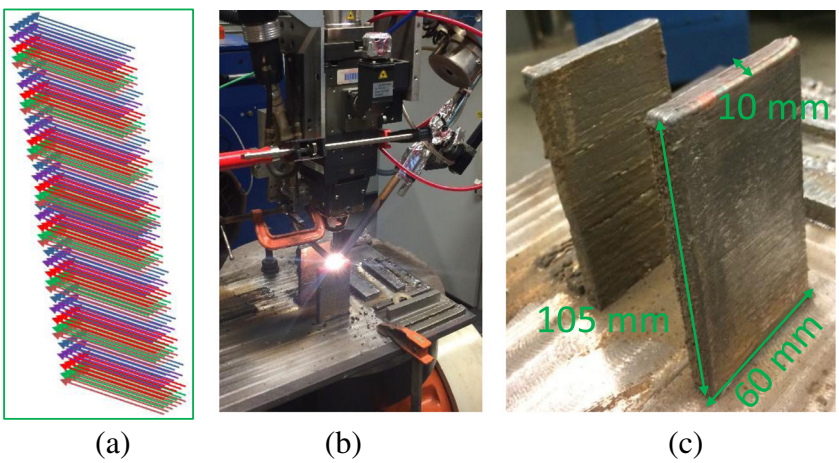

Fig. 4 **a** Tool path for a block using the raster pattern. **b** Process of building a block. **c** As-built blocks (105 mm high, 60 mm long, and 10 mm thick)

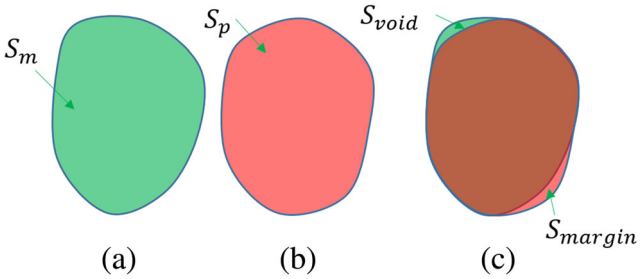

Fig. 5 **a** The original CAD contour. **b** The as-built contour. **c** The overlap between the original CAD contour and the as-built contour

top or from inside to outside [15], a series of enclosed free-form contours are obtained. Figure 5a shows the schematic of the enclosed free-form contour. S_m is the original CAD contour shown in Fig. 5a, and S_p is the as-built contour shown in Fig. 5b. Figure 5c shows the overlap between S_m and S_p. S_{margin} is the margin area on the as-built contour compared to the original CAD contour. It can be expressed as $S_{\text{margin}} = S_m - S_p \cap S_m$. S_{margin} has to be machined when a high shape accuracy is needed. S_{void} is the void area on the as-built contour compared to the original CAD contour. It can be expressed as $S_{\text{void}} = S_m - S_p \cap S_m$. S_{void} should be eliminated in order to obtain a shape-qualified component. The fundamental requirement on the tool process planning is that the filling tool paths completely cover the whole contour with a minimum margin. That requirement can be formulated as

$$(S_{void} = 0)\&\&\text{Min}(S_{margin}).$$

Void ratio and margin ratio are defined as S_{margin}/S_m and S_{void}/S_m, respectively.

4.2 Proposed method for filling

As can be concluded from building up the blocks, the start-and-stop of deposition made the surfaces at the two ends rough, where extra material had to be added for post-machining. It also had a stair-step effect along the boundary when building free-form contour as shown in Fig. 7g. To get a good surface and minimize the amount of additional material, the number of start-and-stops of deposition along the contour should be minimized. Traditionally, the longest straight line inside the contour was chosen as the vector to fill the contour. This method resulted in start-and-stops of deposition existing along the whole contour (see Fig. 6a). Another filling method proposed in ref. [16] filled the con-

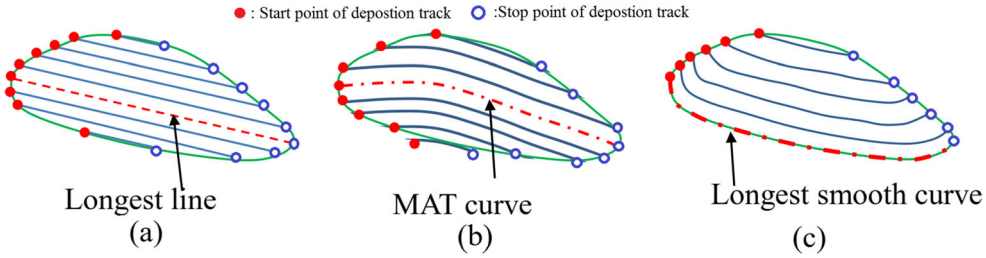

Fig. 6 **a** Filling contour using longest line as vector. **b** Filling contour from MAT curve toward outside [16]. **c** Proposed filling pattern

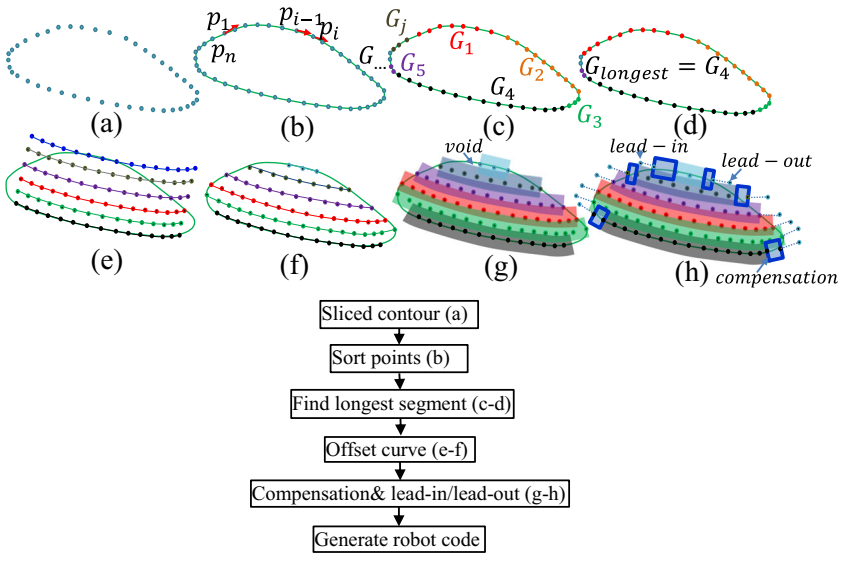

Fig. 7 Procedure of the proposed process planning method

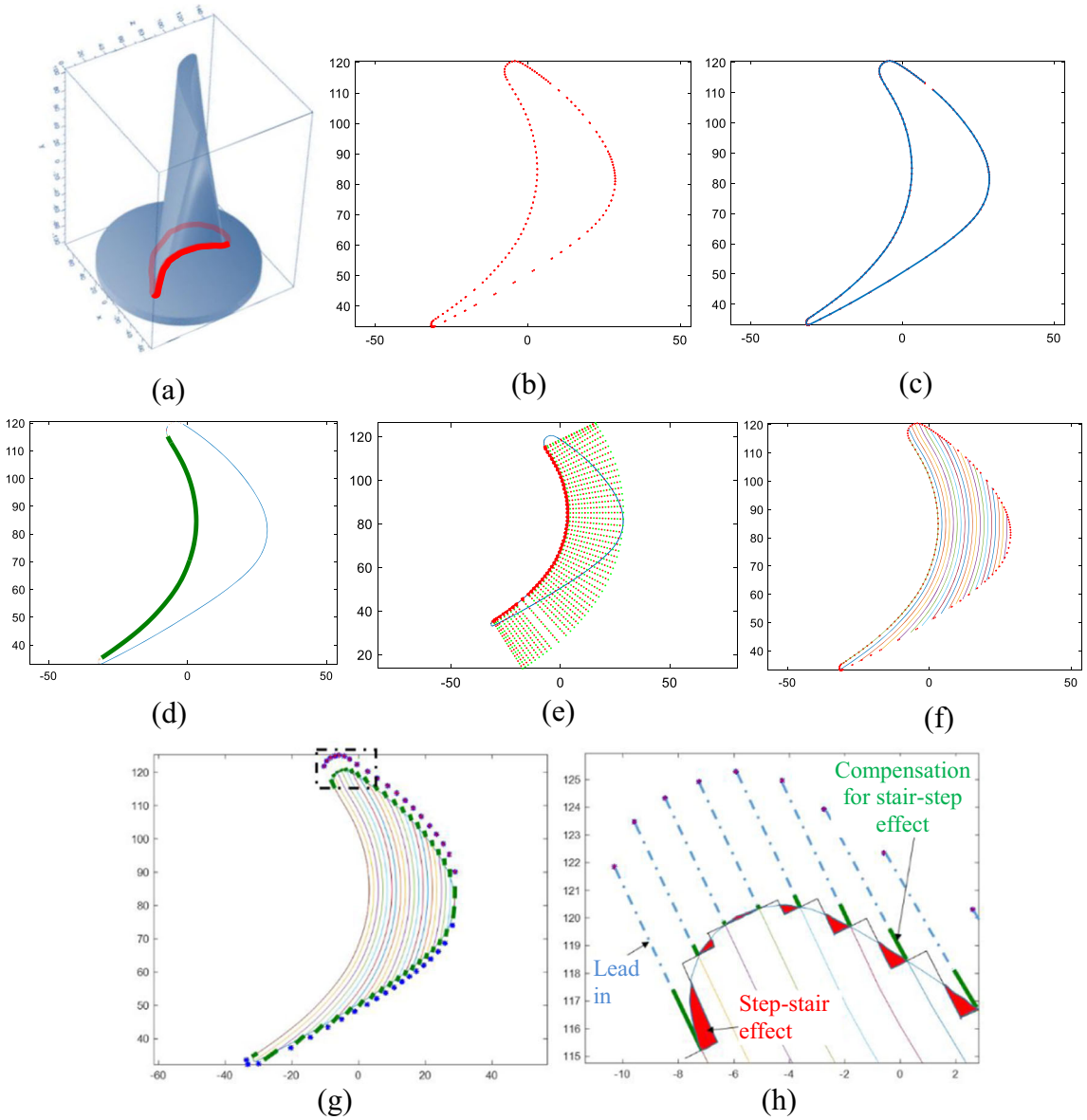

Fig 8 Process planning for a free-form contour sliced from a blade. **a** CAD model of the blade. **b** Sliced contour that consists of a sequence of unsorted points. **c** Sorted points along the contour. **d** Extracted longest smooth curve (the curve in green color). **e** Result of offsetting the extracted curve. **f** Tracks that fully cover the contour. **g** Compensation for step-stair effect and determination of lead-in/out point. **f** A zoom-in view of **g**

tour from a MAT curve toward the outside. This method also resulted in start-and-stops of deposition existing along the whole contour (see Fig. 6b).

In this study, a long smooth curve was extracted from the boundary curve. The contour was filled by offsetting the smooth curve with a certain y offsetting until it completely

Fig. 9 **a** As-built contour without elongation for step error. **b** As-built contour with elongation for step error

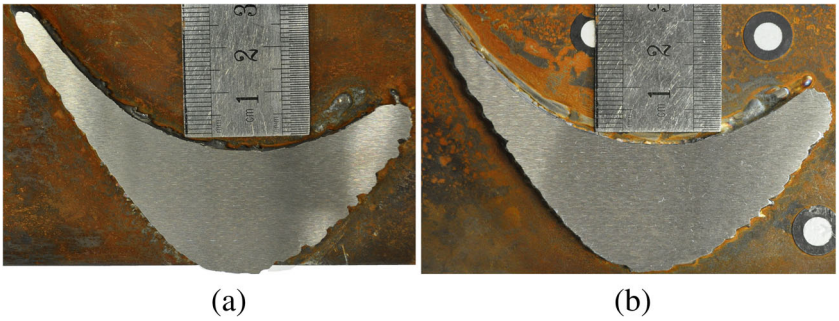

Fig. 10 **a** A top view of the as-built contour without compensation after machining the horizontal surface. **b** A top view of the as-built contour with compensation after machining the horizontal surface

covered the contour. In this way, no start-and-stop of deposition existed along the extracted curve (see Fig. 6c). The surface along the extracted curve was smooth with no need to add material for post-machining. This method was significantly effective for walled free-form structures like propeller, blade, and impeller, because the extracted smooth curve could be very long. Consequently, a large fraction of the surface was smooth and needed a very small amount of additional material for post-machining.

The schematic presentations of the proposed filling process are shown in Fig. 7. It consists of five steps that are detailed as follows:

1. Sort the points

As shown in Fig. 7a, the original contour consists of a sequence of unsorted points. The points are sorted by seeking the nearest point as the next point. Figure 7b shows the sorted points $p_1, p_2, p_3 \ldots p_n$ along the contour.

2. Split the contour

To find the longest smooth curve, the sorted points are split by grouping the points under the condition that the tangential direction changed per unit is less than a threshold, and the tangential angle between the end point and start point is less than a threshold. The threshold was set to be 15° in this study. As seen in Fig. 7b, a point p_1 on the contour is chosen as the start point of group G_1. Its next point is grouped into G_1 if

$$\left|\alpha_{p_{i-1}} - \alpha_{p_i}\right| < \varepsilon_{gradient}, \quad (1)$$

$$\left|\alpha_{p_{i-1}} - \alpha_{p_1}\right| < \varepsilon_{total}, \quad (2)$$

$(i = 2, 3, 4 \ldots n)$. n is the number of points on contour. α_{p_i} is the tangential angle of point p_i, $\alpha_{p_i} = atan\left(\frac{y_{p_{i+1}} - y_{p_{i-1}}}{x_{p_{i+1}} - x_{p_{i-1}}}\right)$ $(i = 3, 4 \ldots n-1)$. For i = 1 and n, $\alpha_{p_1} = \alpha_{p_2}$ and $\alpha_{p_n} = \alpha_{p_{n-1}}$. $\varepsilon_{\text{gradient}}$ is the threshold of tangential angle gradient, and $\varepsilon_{\text{total}}$ is the threshold of tangential angle between the end point and the start point. If one of the two equations (Eqs. 1 and 2) is not met, this group G_1 stops growing. The next group G_2 starts growing with p_i as the initial point. The grouping process proceeds until all points on the contour are grouped. Figure 7c shows the detected groups $G_1, G_2 \ldots G_j$. The above steps group the points in a line while the contour is a loop, so at the last step, the first group G_1 and the last group G_j are grouped, if they meet the equations (see Fig. 7c, d).

3. Offset the longest curve to cover the contour

The longest curve is found by calculating the lengths of the split curves (see Fig. 7d). To fill the contour, the longest curve is offset by moving individual points along their normal directions (see Fig. 7e). For offsetting curves that go outside of the boundary, the outside part is trimmed off. For those with start or end points inside the boundary, the start/end points of the curves are extended to the boundary along the tangential direction (see Fig. 7f).

4. Elongate the curve to compensate for the stair-step error

Figure 7g shows the deposition tracks following the filling paths. Voids exist at the start-and-stop points of some tracks. To compensate for the voids, the start-and-stop points of deposition tracks are extended along the tangential direction until the voids disappear (see Fig. 7h). The

Table 3 Margin and void ratios at three cross sections for as-built shape with/without elongation

Elongation for step error	Area type	Cross-section 1	Cross-section 2	Cross-section 3	Averaged value
Without	Margin	11.04%	10.20%	10.98%	10.74%
	Void	4.32%	4.80%	4.17%	4.43%
With	Margin	12.19%	12.63%	12.47%	12.43%
	Void	0.86%	0.99%	0.94%	0.93%

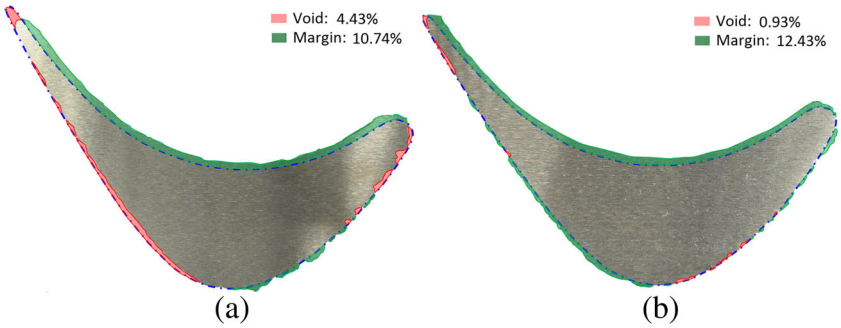

Fig. 11 Comparison between the as-built one and the original CAD model. **a** Without compensation and **b** with compensation (green area is margin area while red area is void area)

voids are compensated based on local geometries instead of considering the machining allowance on the original model. This compensation saves material at the smooth places where only a small amount of additional material is needed for post-machining.

5. Generate the robot code in MATLAB

For each track, the lead-in and lead-out points are determined by extending the start-and-stop point along their tangential directions with a lead-in/lead-out distance (see Fig. 6h). The TCP position and orientation of the laser head at a point is *TCPpi = [xpi, ypi, zpi, api, bpi, cpi, E1pi, E2pi]*. The command to reach this position and orientation can be generated by *fprintf(fid, 'LIN{E6POS: X %4.4f, Y %4.4f, Z %4.4f, A %4.4f, B %4.4f, C %4.4f, E1%4.4f, E2%4.4f} C_DIS\n', TCPpi)*. *fid* is the defined file handle *fid = fopen(['name of src file', '.txt'],'wt')*. The command for laser/wire control is defined in the sub-function as

$$fprintf\left(\text{fid},\ 'LASERON()\%\text{n}'\right); fprintf\left(\text{fid},\ 'WIREON()\%\text{n}'\right);$$

$$fprintf\left(\text{fid},\ 'LASEROFF()\%\text{n}'\right); fprintf\left(\text{fid},\ 'WIREOFF()\%\text{n}'\right);$$

5 Building cases

5.1 Building case in 2D: a free-form enclosed contour

A free-form enclosed 2D contour sliced from a blade was built using the proposed process planning method. As shown in Fig. 8a, the model of the blade was sliced from bottom to top with a z increment of 0.5 mm. A contour near the bottom is shown in Fig. 8b. Figure 8c–h shows the result of each step described in Sect. 4.2. The contour was built 8 mm high without and with elongation, respectively. The processing parameters in Table 1 were used for the building processes. The as-built shapes are shown in Fig. 9. The sideway surfaces along the extracted curve were smooth as expected. To compare the as-built shapes with the original CAD contour, the as-built shapes were machined at the horizontal surfaces to three different depths. The cross section at each depth was imaged as shown in Fig. 10. The margin and void ratio defined in Sect. 4.1 were calculated, respectively, and shown in Table 3.

The averaged void ratio and margin ratio of the as-built shape without compensation were 4.43 and 10.74%, respectively. Whereas for the one with compensation, the averaged void ratio and margin ratio were 0.93 and 12.43%,

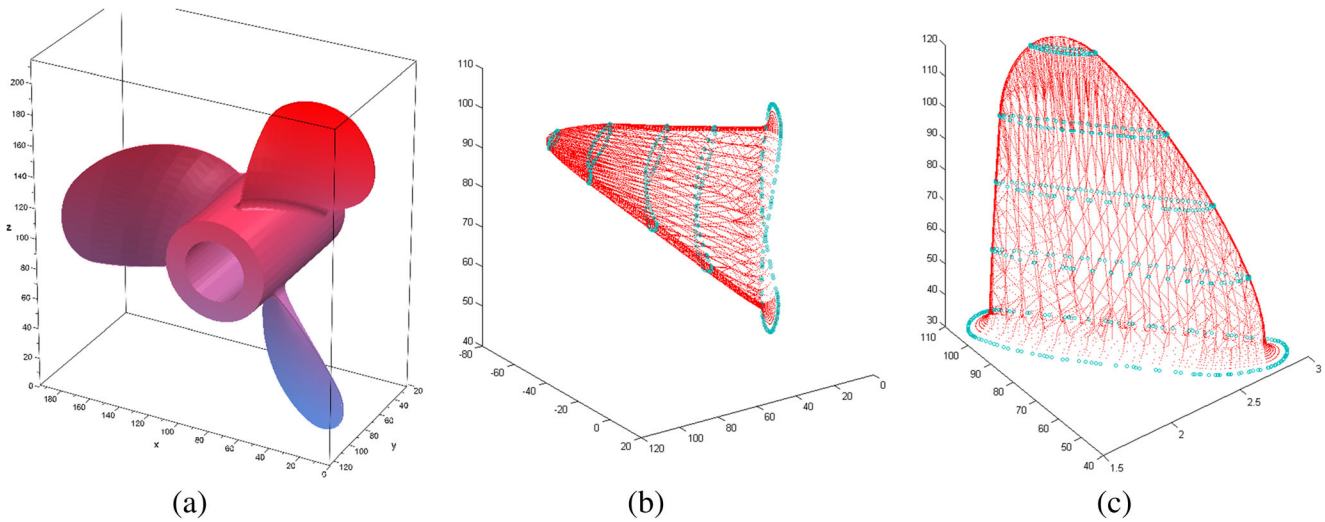

Fig. 12 **a** Original CAD model of the propeller. **b** Sliced contours of a blade in Cartesian coordinate. **c** Contours mapped to cylindrical coordinate

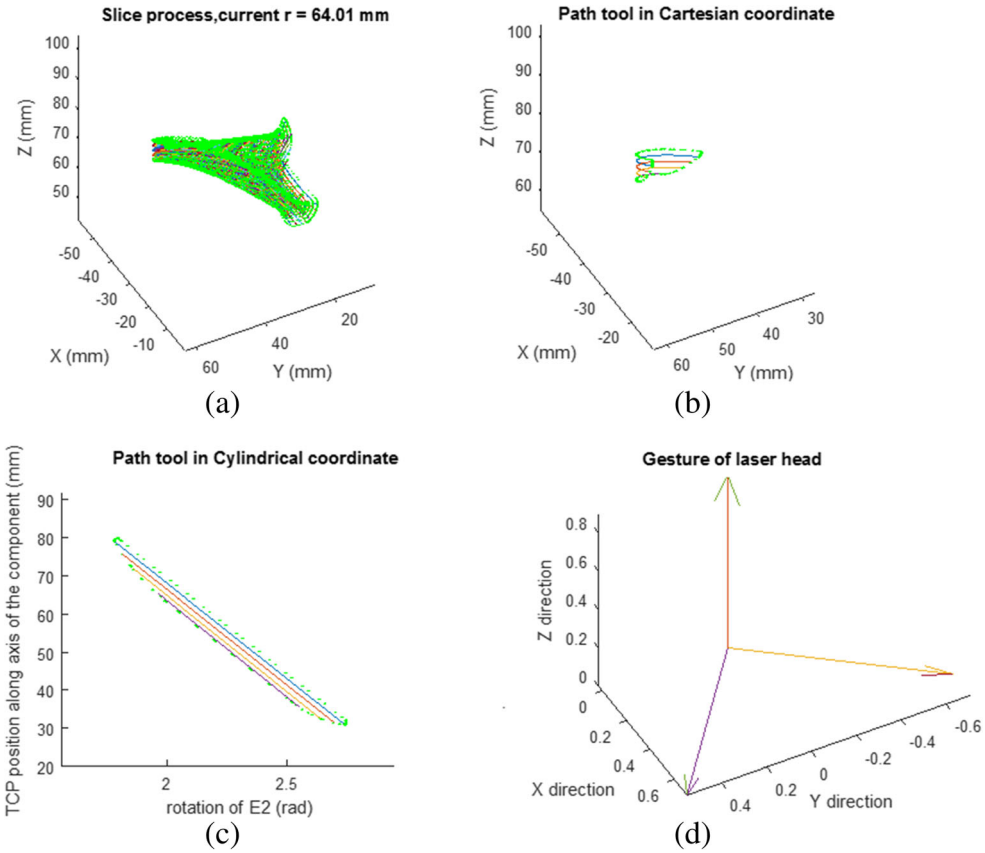

Fig. 13 Process planning process for a propeller. **a** Process of cylindrically slicing the blade from inside to outside. **b** Tracks for the sliced contour in Cartesian coordinate. **c** Tracks for the sliced contour in cylindrical coordinate. **d** Orientation of the laser head

respectively. The proposed compensation method at the start-and-stop points of tracks effectively decreased the void ratio with a small increase in margin void. As can be seen from the overlapped cross sections in Fig. 11, the red area represents the void area along the start-and-stop points. To further decrease the void area to zero, more compensation was needed at the start-and-stop points of tracks. The high margin ratios (10.74, 14.43%) were mainly from the first track (green area on the top of the cross section). In this study, the first track was aligned with the extracted curve such that half of the deposited material became margin area during the first track. In the future study, preventing this void will be investigated by offsetting the first track toward the inside.

5.2 Build case in 3D: a propeller

A propeller was built at the LWMAM system for testing the performance of the developed software. As shown in Fig. 12a, the size of the propeller was 200 × 200 × 50 mm. It consisted of three twisted free-form blades mounted at equal intervals on a cylinder. Following the slicing method described in ref. [15], the overhanging structures (blades) of the propeller were mapped to be at a planar base. Volumes of the blades were transferred from the Cartesian coordinate (see Fig. 12b) to the cylindrical coordinate (see Fig. 12c). The tracks for filling the sliced contours in the cylindrical coordinate were planned by the proposed filling pattern. To save slicing time, only one blade was sliced.

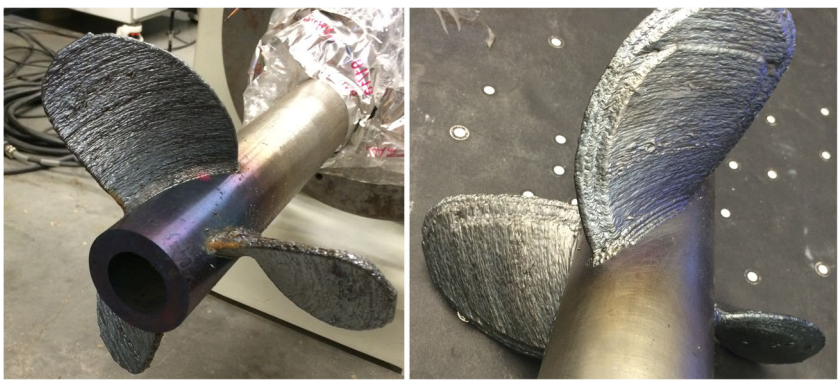

Fig. 14 Two views of the as-built propeller

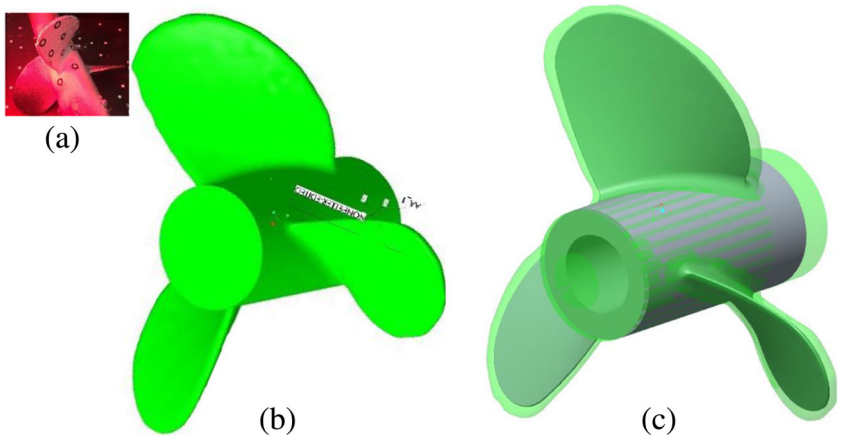

Fig. 15 **a** Propeller during the 3D scanning process, **b** scanned 3D profile of the as-built propeller, and **c** comparison between the scanned profile of the as-built propeller and the original CAD model

Figure 13 shows the cylindrical slicing process for a blade, the tracks in the Cartesian coordinate, the tracks in the cylindrical coordinate, and the orientation of the laser head. To completely eliminate the voids in the as-built propeller, an extra compensation 4 mm long was added and combined with the compensation for stair-step effect at the start-and-stop points of tracks. The propeller was built with the parameters in Table 1. The building process took 3.5 h. Figure 14 shows the as-built propeller.

In order to calculate the margin ratio and void ratio of the as-built propeller, a 3D scanning tool (scanning resolution of 0.98 mm) along with a data processing software Geomagic Studio 10 was used to reconstruct the 3D profile of the as-built propeller. Figure 15b shows the scanned profile of the as-built propeller after a repair in Geomagic Studio 10. By aligning the shafts and rotating the scanned propeller for the maximum overlap with the original CAD model (see Fig. 15c), the original CAD model could be completely inside the scanned profile; that is, the void ratio was zero. The margin ratio was 10.56%. Therefore, by machining 10.56% margin material of the as-built propeller, a propeller geometrically identical to the original CAD model could be obtained. Successful buildup of the propeller indicated that the proposed process planning strategy had the ability to additively fabricate intricate solid free-form components with no void and a small margin volume.

6 Conclusions

LWMAM is a promising additive manufacturing technology that is well suited to build from various materials near net shape mid- to large-size complex components that have a high deposition rate and high material usage. This paper details the development of a MATLAB-based process planning software specific to LWMAM that consists of modules for volume slicing, contour filling, track trimming/elongating, stair-step effect compensation, and post-processing. It was successfully applied to build free-form contours and a propeller. The development of this software could be concluded as the following:

(1) The key issues involved in the LWMAM process were identified by building up a prismatic block. The corresponding strategies were proposed and successfully tested including adding lead-in/out distance, adjusting the laser power, and pulling away the laser head with a high speed at the end of tracks.
(2) The free-form solid contour was filled by offsetting a smooth curve extracted from the boundary curve such that no start-and-stop action existed along the extracted curve. The surface on the side of the extracted curve was smooth and could significantly save from adding extra material for post-machining/milling.
(3) The software compensated for the stair-step effect by elongating the individual tracks. This method followed the local geometry instead of offsetting the boundary of the original model. It saved from adding extra material for post-machining/milling.
(4) This MATLAB-based software provided the flexibility for different control strategies and could be easily extended for application with arc wire-feed MAM, electron wire-feed MAM, laser wire-feed MAM, and laser powder-feed MAM.

Acknowledgments The authors would like to thank Mr. Andrew Socha at the Research Center for Advanced Manufacturing at SMU for his assistance in this research. The financial support of National Science Foundation of USA under the Grant IIP-1539853 is acknowledged.

References

1. Frazier WE (2014) Metal additive manufacturing: a review. J Mater Eng Perform 23(6):1917–1928
2. Ding D et al (2015) Wire-feed additive manufacturing of metal components: technologies, developments and future interests. The International Journal of Advanced Manufacturing Technology 811–4:465–481

3. X. Wang, X. Gong, K. Chou (2016) Review on powder-bed laser additive manufacturing of Inconel 718 parts, Proc Inst Mech Eng Part B J Eng Manuf 954405415619883. https://doi.org/10.1177/0954405415619883
4. Liu S, Liu W, Harooni M, Ma JJ, Kovacevic R (2014) Real-time monitoring of laser hot-wire cladding of Inconel 625. Opt Laser Technol 62:124–134
5. Wang X, Chou K (2017) Electron backscatter diffraction analysis of Inconel 718 parts fabricated by selective laser melting additive manufacturing. JOM 69:402–408. https://doi.org/10.1007/s11837-016-2198-1
6. Baufeld B, Brandl E, Van der Biest O (2011) Wire based additive layer manufacturing: comparison of microstructure and mechanical properties of Ti–6Al–4V components fabricated by laser-beam deposition and shaped metal deposition. J Mater Process Technol 211(6):1146–1158
7. Wang X, Gong X, Chou K (2015) Scanning speed effect on mechanical properties of Ti-6Al-4V alloy processed by electron beam additive manufacturing. Procedia Manuf 1:287–295. https://doi.org/10.1016/j.promfg.2015.09.026
8. Wang X, Chou K (2015) Residual stress in metal parts produced by powder-bed additive manufacturing processes, in: Int. Solid Free. Fabr. Symp., Austin, Texas, USA pp. 1463–1474)
9. Ding Y, Zhang X, Kovacevic R (2016) A laser-based machine vision measurement system for laser forming. Measurement 82:345–354
10. Fu, Youheng, et al. (2017) Investigation of mechanical properties for hybrid deposition and micro-rolling of bainite steel. J Mater Process Technol
11. Wang X, Keya T, Chou K (2016) Build height effect on the Inconel 718 parts fabricated by selective laser melting. Procedia Manuf 5:1006–1017. https://doi.org/10.1016/j.promfg.2016.08.089
12. Ding Y, Warton J, Kovacevic R (2016) Development of sensing and control system for robotized laser-based direct metal addition system. Additive Manufacturing 10:24–35
13. Ding Y, Huang W, Kovacevic R (2016) An on-line shape-matching weld seam tracking system. Robot Comput Integr Manuf 42:103–112
14. Akbari, Meysam, Yaoyu Ding, and Radovan Kovacevic (2017) Process development for a robotized laser wire additive manufacturing. ASME 2017 12th International Manufacturing Science and Engineering Conference collocated with the JSME/ASME 2017 6th International Conference on Materials and Processing. American Society of Mechanical Engineers
15. Ding Y, Dwivedi R, Kovacevic R (2017) Process planning for 8-axis robotized laser-based direct metal deposition system: a case on building revolved part. Robot Comput Integr Manuf 44:67–76
16. Ding D et al (2015) A practical process planning methodology for wire and arc additive manufacturing of thin-walled structures. Robotics and Computer-Integrated Manufacturing 34:8–19
17. Cao J, Gharghouri MA, Nash P (2016) Finite-element analysis and experimental validation of thermal residual stress and distortion in electron beam additive manufactured Ti-6Al4V build plates. J Mater Process Technol 237:409–419
18. Ding Y, Kovacevic R (2016) Feasibility study on 3-D printing of metallic structural materials with robotized laser-based metal additive manufacturing. JOM 68(7):1774–1779
19. Syed WUH et al (2005) Effects of wire feeding direction and location in multiple layer diode laser direct metal deposition. Appl Surf Sci 248:518–524
20. Yang G et al (2017) Decreasing the surface roughness of aluminum alloy welds fabricated by a dual beam laser. Mater Des 127:287–296
21. Yang G, Ma J, Carlson B, Wang H-P, Kovacevic R (2017) Effect of laser beam configuration on microstructure evolution and joint performance in laser joining AA 6111 panels. Mater Des 123:197–210
22. Zhang YM et al (2002) Automated system for welding-based rapid prototyping. Mechatronics 12.1:37–53
23. Ding D et al (2016) Towards an automated robotic arc-welding-based additive manufacturing system from CAD to finished part. Comput Aided Des 73:66–75
24. Song Y-A et al (2005) 3D welding and milling: part I—a direct approach for freeform fabrication of metallic prototypes. International Journal of Machine Tools and Manufacture 45.9:10571062
25. Dwivedi R, Kovacevic R (2004) Automated torch process planning using polygon subdivision for solid freeform fabrication based on welding. Journal of Manufacturing Systems 23.4:278–291
26. Ren L et al (2008) Process planning strategies for solid freeform fabrication of metal parts. Journal of Manufacturing Systems 274:158–165
27. Ruan J, Eiamsa-ard K, Liou FW (2005) Automatic process planning and toolpath generation of a multiaxis hybrid manufacturing system. Journal of manufacturing processes 71:57–68
28. Dwivedi R, Kovacevic R (2006) An expert system for generation of machine inputs for laser-based multi-directional metal deposition. Int J Mach Tools Manuf 46(14):1811–1822
29. Kottman M, Zhang S, McGuffin-Cawley J, Denney P, Narayanan BK (2015) Laser hot wire process: a novel process for near-net shape fabrication for high-throughput applications. JOM 67(3):622–628
30. Dunlavey MR (1983) Efficient polygon-filling algorithms for raster displays. ACM Trans Graph 2:264–273
31. Farouki R et al (1995) Process planning with offset curves for layered fabrication processes. J Manuf Syst 14:355–368
32. Ren F et al (2009) Combined reparameterization-based spiral toolpath generation for five-axis sculptured surface machining. Int J Adv Manuf Technol 40:760–768
33. Chiu W et al (2006) Toolpath generation for layer manufacturing of fractal objects. Rapid Prototyp J 12:214–221